ELSEVIER

Contents lists available at ScienceDirect

# Catalysis Today

journal homepage: www.elsevier.com/locate/cattod





# From deposited metal precursors to supported atoms or nanoparticles

John R. Regalbuto <sup>b,\*</sup>, Edward Chandler <sup>a</sup>, Chigozie Ezeorah <sup>b</sup>, Alaba Ojo <sup>b</sup>, Nathan Thornburg <sup>b</sup>, Mikayla Romero <sup>c</sup>, Hien Pham <sup>c</sup>, Abhaya Datye <sup>c</sup>, Tae-Yeol Jeon <sup>d</sup>, B. Frank Gupton <sup>a</sup>, Christopher T. Williams <sup>b</sup>

- <sup>a</sup> Dept. of Chemical Engineering, Virginia Commonwealth University, Richmond, VA, USA
- <sup>b</sup> Dept. of Chemical Engineering, University of South Carolina, Columbia, SC, USA
- <sup>c</sup> Dept. of Chemical and Nuclear Engineering, University of New Mexio, Albuquerque, USA
- <sup>d</sup> Pohang Accelerator Laboratory, Nam-gu, Pohang, Gyeongbuk, South Korea

#### ARTICLE INFO

# Keywords: Strong electrostatic adsorption Single atom catalysts Drying Supported metal nanoparticles Surface tension Agglomeration

#### ABSTRACT

Strong Electrostatic Adsorption is a simple method to prepare highly dispersed supported metals. However, the minimum size of nanoparticles produced with gas phase reductions after SEA is typically about 1–2 nm. Alternative methods are explored to further decrease particle size, that is, to control the agglomeration of adsorbed precursors into nanoparticles, clusters, or isolated atoms. Three alternative methods have been employed to synthesize carbon supported Pt with higher dispersion than can be prepared by a "standard" method of strong electrostatic adsorption of charged Pt precursors followed by gas phase hydrogen reductions. First, gas phase reduction is replaced by a liquid phase reduction with hydrazine. Second, carbon black surfaces are oxidized to render them more hydrophilic and decrease the degree of agglomeration of Pt precursors after drying. The third method involves a switch of solvent from water to a solvent -acetone - which wets the carbon surface. The ensuing samples comprised of isolated atoms, clusters, and nanoparticles were characterized by high sensitivity XRD and z-contrast STEM imaging.

# 1. Introduction

An advance in the understanding of heterogeneous catalyst synthesis has been achieved with the decades-long study of "strong electrostatic adsorption" (SEA) which was inspired by the pioneering work of Brunelle [1] and Schwarz [2–4]. Based on electrostatic interaction between metal catalyst precursors in the form of charged metal coordination complexes, with oppositely charged surfaces achieved by controlling the aqueous impregnation solution pH relative to the point of zero charge (PZC) of the support material, SEA has been shown to yield ultrasmall (sub 2 nm) nanoparticles over oxide and carbon surfaces [5–7]. In contrast, with incipient wetness/dry impregnation (DI) preparations, there is no interaction of the metal complex with the support surface. The metal remains in solution and as drying occurs, is brought to the drying surfaces where it agglomerates, typically resulting in larger particles with broader size distribution than found in SEA-derived catalysts. The difference between these two methods is illustrated in Fig. 1.

The small size and tight size distributions of SEA-prepared nanoparticles possess inherent advantages vis-à-vis DI-derived in applications such as catalysis. However, one current limitation of the method is the inability to synthesize nanoparticles smaller than  $\sim\!1\text{--}2$  nm. Using calcination or reduction pretreatments, it is possible to increase the size of SEA-derived particles size [8,9], however, a systematic exploration of methods to control the degree of agglomeration of adsorbed precursors into nanoparticles, smaller clusters, or even isolated atoms has yet to be made. That is the purpose of the methods whose preliminary results are shown in this work.

The knowledge gap being addressed is depicted in Fig. 2. That metal precursors adsorb with one or two hydration sheaths intact and that the maximum uptake of precursors is a close packed layer of these complexes (top of Fig. 2a) has been firmly established by both direct [10] and indirect [11,12] measurements. The ultrasmall nanoparticles yielded from this monolayer or sub-monolayer of precursors is depicted in the bottom sketch of Fig. 2a, and what is missing is the knowledge of the mechanism by which, during drying and pretreatment, the precursors assemble into nanoparticles.

The hypothesis of this work is suggested by the image of a just-dried sample of Pt hexachloride precursors on a thin sliver of alumina, seen in

E-mail address: regalbuj@cec.sc.edu (J.R. Regalbuto).

<sup>\*</sup> Corresponding author.

J.R. Regalbuto et al. Catalysis Today 431 (2024) 114556

the z-contrast image of Fig. 2b. The precursors are seen to be agglomerated, and while this can be attributed to the reducing environment of the electron beam interacting with this insulating support, another interpretation of the image is that the deposited material is stable in the beam, and the precursors had agglomerated during the drying step. The driving force for this agglomeration is surface tension. As drying occurs, the predominant force between precursors and support can no longer be electrostatic, as the liquid phase disappears. We hypothesize that surface tension replaces electrostatics as the predominant force during drying. The remaining water in the system, including the hydration sheaths surrounding each precursor, form into nanodroplets as depicted in the sketch of SEA in Fig. 1, and it is the size of these nanodroplets that give rise to the minimum size of SEA-derived nanoparticles.

The central hypothesis of precursor agglomeration caused by surface tension led to the exploration of three alternative methods to restrict agglomeration:

- A change of reduction chemistry: reducing in the liquid phase. Liquid
  phase reduction of metal precursors is commonly employed in the
  synthesis of electrocatalysts [13–15]. Reducing precursors in the
  liquid phase circumvents agglomeration by surface tension. In this
  case, the precursors reduced in the liquid phase will be those electrostatically adsorbed as monolayers or sub-monolayers on the support surface.
- 2. A change of surface chemistry: controlling the hydrophilicity of carbon supports by surface oxidation. The hypothesis is to minimize the volume of agglomerated nanodroplets by making the carbon surface more hydrophilic. A hydrophobic carbon, characterized by a high PZC value, will be successively oxidized and the trends in the

- metal agglomeration after drying and reduction will be characterized as the carbon PZC is lowered.
- 3. Switching the solvent: substituting water for a wetting solvent. The idea here is to use the solubilizing ability of water to dissolve the metal precursor, but to switch the solvent to one that has a higher dipole moment, so as to displace the hydration layers, and that also has low surface tension and prefers to wet support surfaces. In aqueous acetone solutions, for example, it is known that an excess of acetone breaks up the hydrogen bonding of water [16]. This method will be termed "switched solvent synthesis," or SwiSS.

Results for these three alternate synthesis methods are illustrated in this work using Pt precursors over two types of carbon support. Scanning transmission electron microscopy and high sensitivity powder XRD have been employed to characterize nanoparticle size resulting from each synthesis variation.

#### 2. Materials and methods

#### 2.1. Materials

The carbons employed for this study were Vulcan VXC-72 (total specific surface area  $223 \text{ m}^2/\text{g}$ , micropore surface area  $58 \text{ m}^2/\text{g}$ ), purchased form the Fuel Cell Store, and Ketjen black EC-300 J (KB300J, total specific surface area  $724 \text{ m}^2/\text{g}$ , micropore surface area  $140 \text{ m}^2/\text{g}$ ) was purchased from Akzo Nobel. The various metal precursors used were platinum (II) dichloride (PtCl<sub>2</sub>), platinum (II) tetraammine nitrate ((NH<sub>3</sub>)<sub>4</sub>Pt(NO<sub>3</sub>)<sub>2</sub>) and dihydrogen platinum (IV) hexachloride (or chloroplatinic acid, H<sub>2</sub>PtCl<sub>6</sub>) were purchased from Sigma Aldrich.

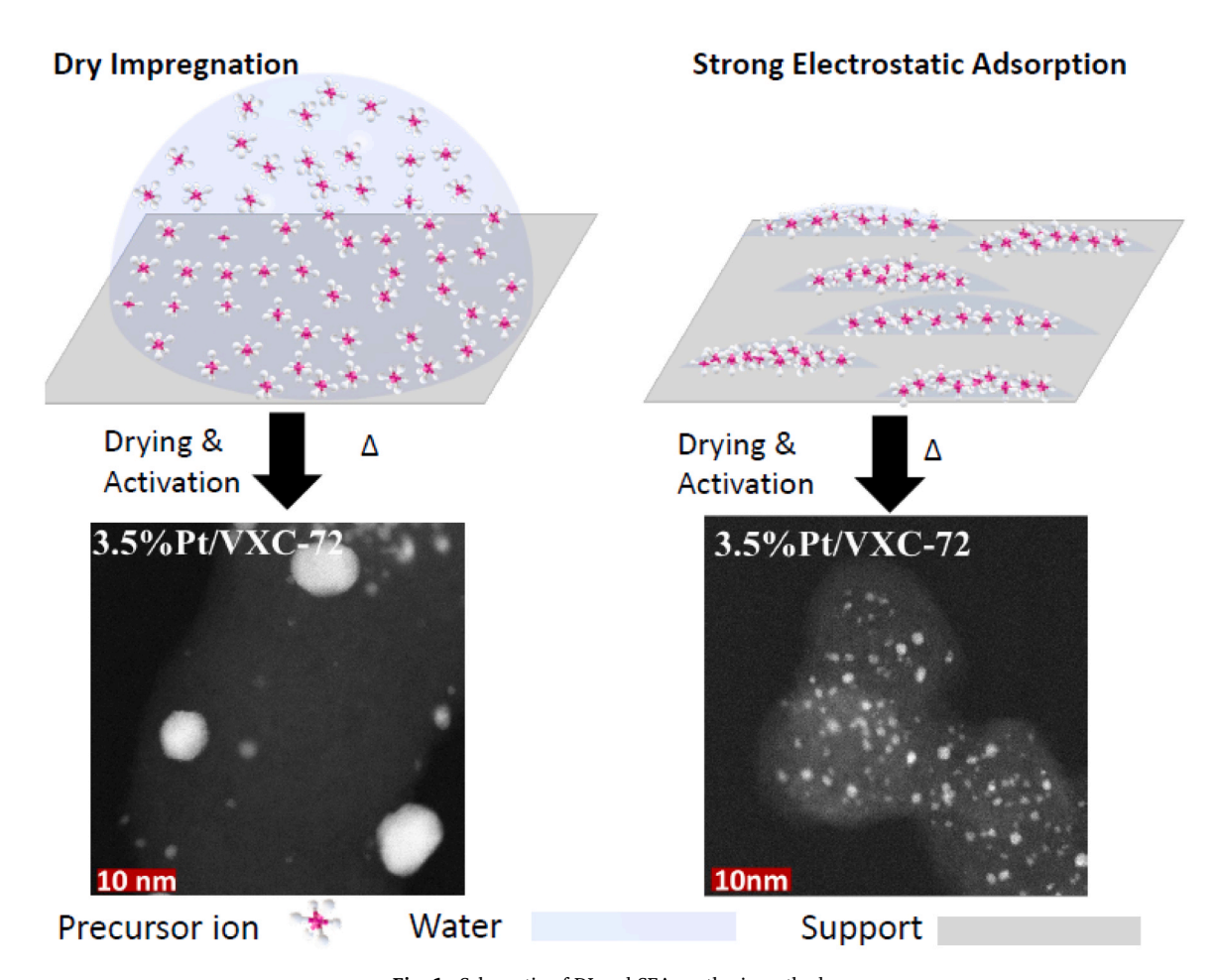


Fig. 1. Schematic of DI and SEA synthesis methods.

#### 2.2. Liquid phase reduction

Hydrazine solution (2.5 mL of aqueous solutions with 100/1 and 10/1 molar ratios of hydrazine/Pt) was quickly added to the mixture solution (25 mL of 114 ppm Pt and 0.1 g of VXC72) containing Pt hexachloride precursor adsorbed at pH 2.9 onto VXC72, and then, stirred for 30 min. The hydrazine solutions of two different molar ratios of hydrazine:Pt were used; 10:1 and 100:1. When dissolved in water, the pH of hydrazine solutions increases rapidly to above 9 by generating hydroxyl ions in water [13,15,17]. In two cases, this was allowed to occur and in another two cases, the pH was kept at the optimal pH for SEA at 2.9. After 30 min contact with the various hydrazine solutions, the solid was filtered, dried at room temperature, and characterized with XRD.

#### 2.3. Carbon surface oxidation

Ketjen Black EC-300 J (KB300J) carbon support with point of zero charge (PZC) 10, was oxidized using varied concentrations and exposure times of nitric acid as described earlier [18]. The exposed support was then thoroughly rinsed using deionized water in a vacuum filter. The rinsing process continues until the pH of the filtrate stabilizes to a steady pH range [18]. The support is dried in an oven, and the new PZC was then checked using a spear tip electrode with a single point measurement using DI water.

Supported nanoparticles were synthesized by strong electrostatic adsorption (SEA) at surface loadings of  $1000~\text{m}^{2/}\text{L}$  using platinum tetraamine nitrate precursor at pH 12, except for the high PZC (10) KB300J for which chloroplatinic acid precursor was used at pH 2.9. Support-precursor solutions were placed on an orbital shaker for 1 h at 120 rpm. The support-solution mixture was then vacuum filtered and dried in a furnace overnight at 50 °C. Following drying, some portions of the powdered samples were reduced in a ceramic boat in a one-inch ID tube furnace at 180 °C in 400 sccm 10% H<sub>2</sub> balanced N<sub>2</sub> for 1 h.

#### 2.4. Switched solvent synthesis (SwiSS)

Platinum nanoparticles were synthesized via SwiSS on VXC-72 with an initial incipient wetness impregnation of aqueous solutions of chloroplatinic acid as illustrated in Fig. 3. Thereafter, the switching solvent, acetone, was added in different molar ratios to water. Lower

acetone to water ratios resulted in thicker pastes while higher ratios yielded thin slurries. These slurries were poured into (homemade) Teflon boats and transferred to a horizontal tube furnace with minimal exposure to ambient air. In the furnace, in a 400sccm flow of  $10\% H_2/$  inert (Ar or  $N_2$ ) the solvent was allowed to evaporate for an hour at room temperature, and then the temperature was ramped at 2 °C/min to  $170\,^{\circ}\text{C}$  and held there for 60 min. After cooling to room temperature in the  $H_2/\text{inert}$  flow the sample was collected for characterization.

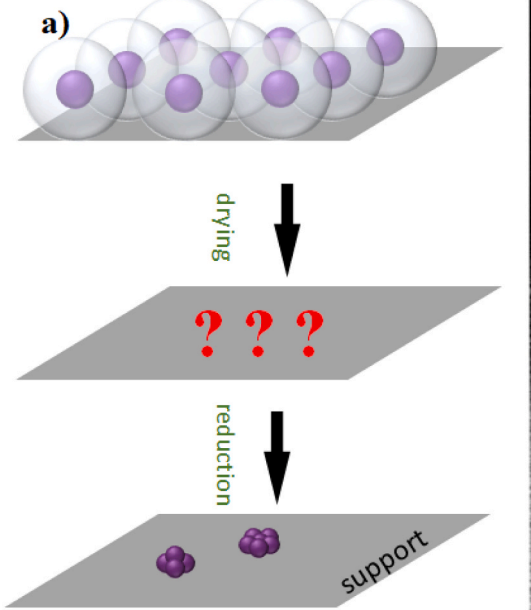
#### 2.5. Characterization

## 2.5.1. High sensitivity powder X-ray diffraction (XRD)

All XRD data was collected using a Rigaku Miroflex Benchtop XRD with a solid state, high sensitivity D/tex detector. The high sensitivity of this detector allows the detection of nanoparticles well below the 2–3 nm limit of scintillation counter detectors; nanoparticles below 1 nm and even down to 0.5 nm have been reliably fit [19–21] with the instrument employed. The fitting software Fityk was used for the analysis of some diffractograms. Particle size was estimated from fitted peaks with the Scherrer equation.

#### 2.5.2. Scanning transmission electron microscopy (STEM)

Samples were mounted on lacey carbon films by dispersing the powder in ethanol and depositing a drop of the suspension on the TEM grid. High Annular dark field (HAADF) images were obtained using a JEOL NeoARM 200 F scanning transmission electron microscope. The microscope is equipped with a spherical aberration corrector, providing a resolution of 0.7 A. The images were recorded using Digital Micrograph software and the sample size was evaluated by using Image J software. For the image analysis of Pt speciation, the Pt species were placed into one of three bins: 1) single atoms,  $N_1$ , 2) dimers and trimers,  $N_{23}$  and 3) clusters with 4 atoms or more were labelled "nanoparticles,"  $N_P$ . The fraction of each entity present was calculated from the number of each species divided by the total number of species; for example, the fraction of single atom species is calculated as  $N_1/(N_1+N_{23}+N_P)$ . STEM particle size histograms and volume average particle size ( $D_v = \Sigma n_i d_i^4/\Sigma n_i d_i^3$ ) were based on nanoparticles only.



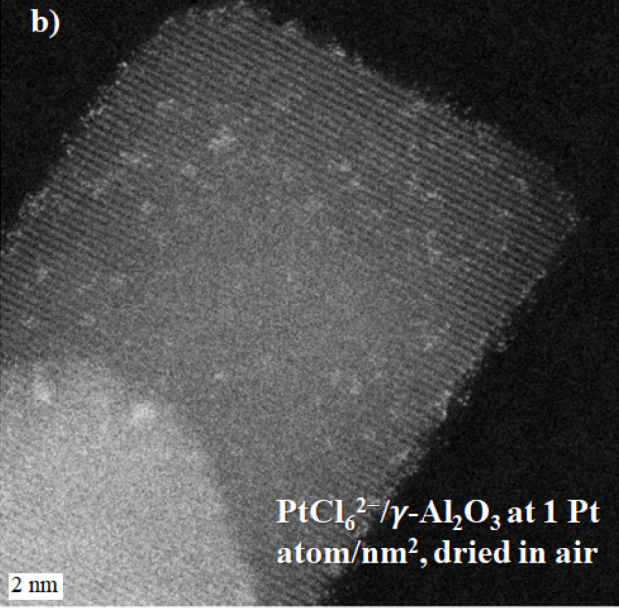


Fig. 2. a) Knowledge gap of drying of precursors, b) image of just-dried sample of Pt hexachloride electrostatically adsorbed onto alumina.

J.R. Regalbuto et al.

Catalysis Today 431 (2024) 114556

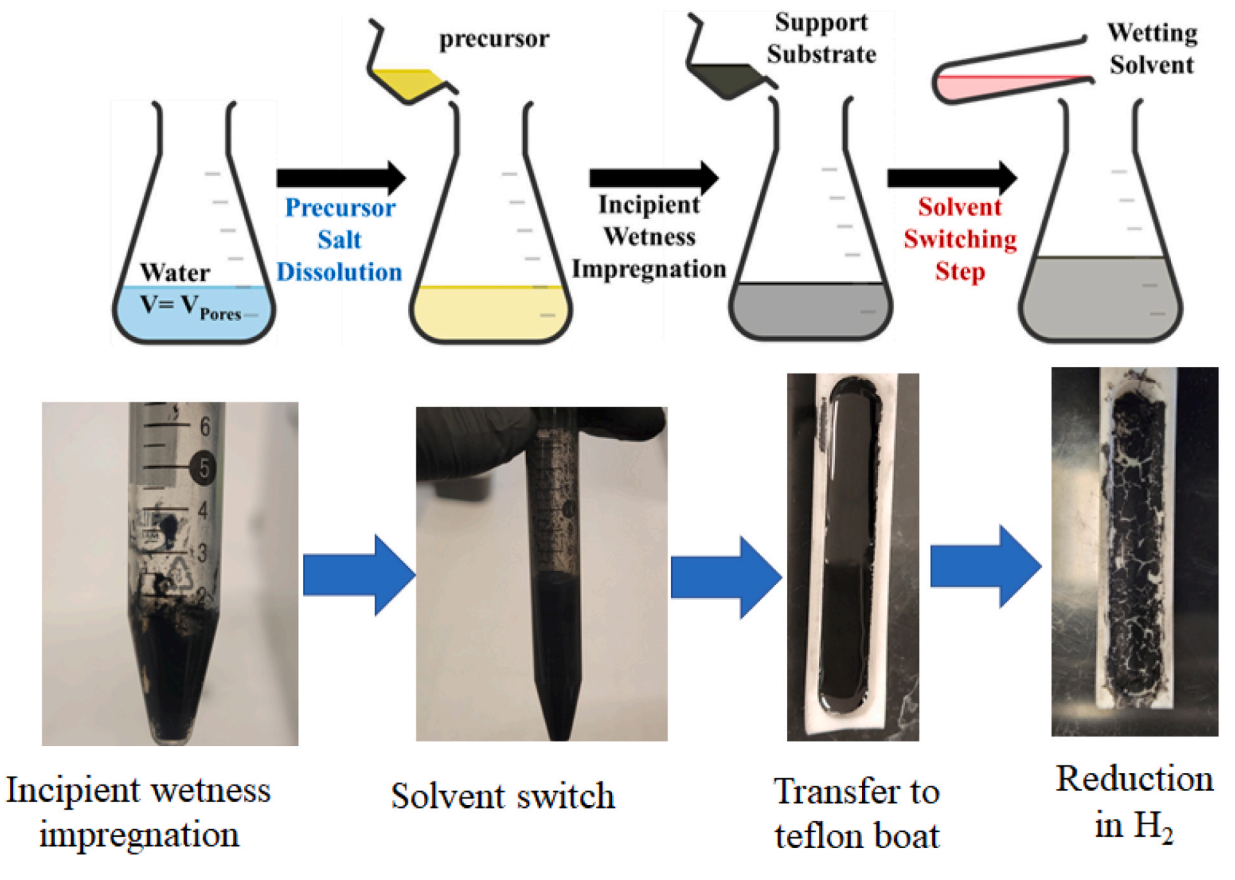


Fig. 3. Steps of switched solvent synthesis.

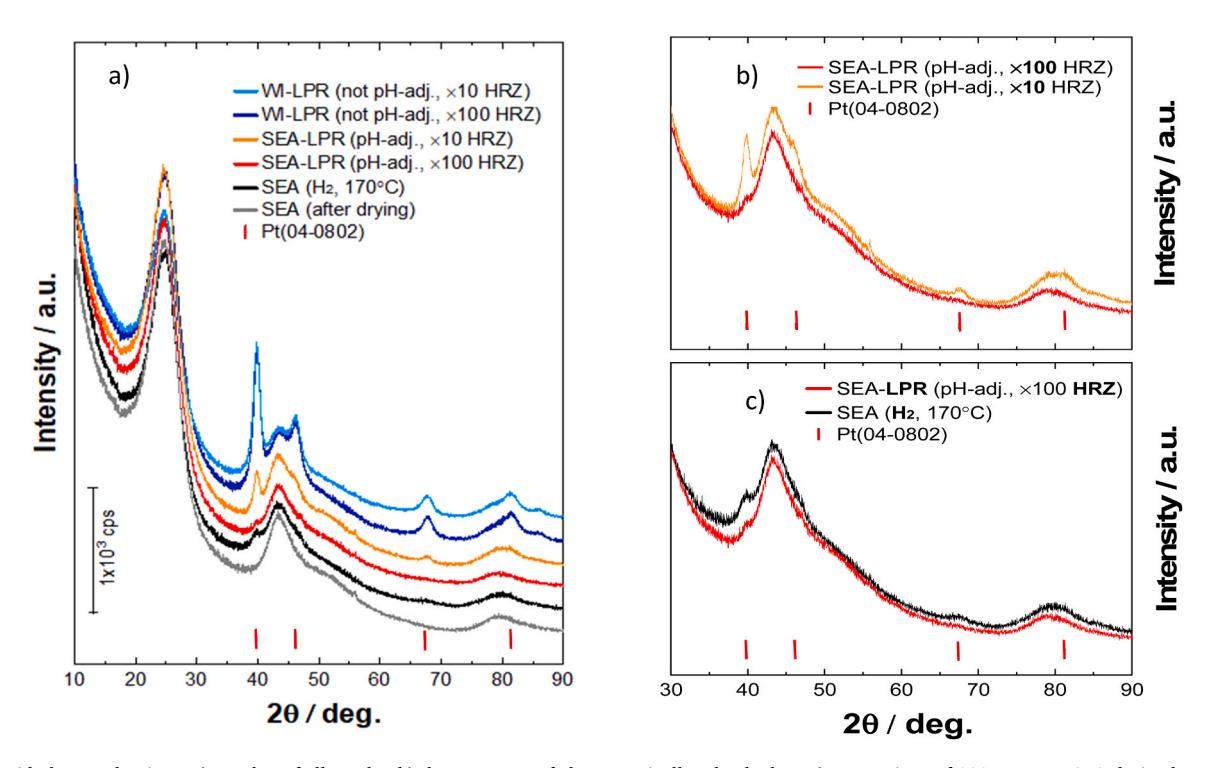


Fig. 4. Liquid phase reductions, a) overlay of all results, b) the two LPRs of electrostatically adsorbed Pt, c) comparison of 100X HRZ to SEA-derived nanoparticles. Hashmarks indicate positions of fcc Pt peaks at 39.8, 46.2, 67.5, and 81.3° 2θ corresponding to Pt (111), (200), (220), and (311).

J.R. Regalbuto et al. Catalysis Today 431 (2024) 114556

#### 3. Results and discussion

#### 3.1. Liquid phase reduction (LPR)

In this series of experiments, anionic Pt hexachloride precursors ([PtCl<sub>6</sub>]<sup>2-</sup>) from chloroplatinic acid were contacted with the unoxidized, PZC 9 VXC-72 support (PZC 9) at the optimal pH of 2.9. Several liquid phase reduction conditions were compared with a traditional gas phase reduction. A composite of XRD results for the set of 2.7 wt% Pt/VXC-72 samples is shown in Fig. 4a. The bottom diffractogram is that of an SEAapplied precursor after drying (with no reduction) and appears equivalent to the support itself. A control sample in which precursors were deposited by SEA at pH 2.9, dried, and then reduced in the gas phase at 170 °C (second pattern from bottom) shows a small Pt (111) peak at  $39.8^{\circ}2\theta$  as well as a rise in the background from  $30-48^{\circ}2\theta$ , which is characteristic of the broad peaks from ultrasmall nanoparticles with Pt oxide shells on metallic cores, consistent with previous observations of ultrasmall (sub-1 nm), ambient-exposed, partially oxidized Pt/carbon samples [19-21]. The top two diffractograms ( light and dark blue patterns in Fig. 4a) are for two liquid-reduced samples in which precursors were applied by SEA at pH 2.9, but after the addition of hydrazine the pH was not controlled and so basified as the hydrazine decomposed. These syntheses are referred to as wet impregnations (WI). The increase in pH caused the Pt to desorb and reduce in the liquid phase, leading to large nanoparticles (about 5.0 - 5.4 nm) for both ratios (10:1 and 100:1) of hydrazine to Pt. These patterns show the maximum intensity of crystalline Pt potentially present in the samples. The integrated intensity of the reduced SEA sample (second from bottom) is much lower than that of either WI sample, which implies that a substantial fraction of the Pt in this sample was below the limit of detection of the (highly sensitive) instrument, which in turn implies that these are either substantially sub-1 nm clusters or isolated atoms. In future work, STEM will be used to fully characterize the distribution of these ultrasmall species.

The middle two patterns in Fig. 4a are for the liquid phase reduction of SEA-adsorbed precursors with 10:1 or 100:1 hydrazine:Pt ratios, with the pH maintained at 2.9. These are shown separately in Fig. 4b. While a significant fraction of Pt crystallizes into large particles (6.1 nm) with 10:1 hydrazine:Pt, there is almost no crystallinity observed in the 100:1 hydrazine:Pt ratio. This is best seen in Fig. 4c, where the 100:1 LPR sample is compared with the SEA sample and is seen to be much less crystalline. That there is no elevated background from 30–48°2 $\theta$  range in the hydrazine-reduced sample implies that the Pt must be present either as ultrasmall clusters or isolated atoms.

Standard liquid phase reductions using strong reducing agents can

produce Pt nanoparticle with the smallest achievable size of 1 - 2 nm in the presence of steric and/or electrostatic stabilizers, which stabilizes growing Pt clusters by providing steric hindrance and/or electronic charge to the metal particles during the reduction process [13–15]. The SEA-LPR sample with 100:1 hydrazine:Pt ratio appears even smaller, and without the use of stabilizers, as seen from the barely discernable crystallinity in Fig. 4. This result suggests that Pt precursors can be reduced in the liquid phase without significant agglomeration after being electrostatically adsorbed onto the support. Once again, future work will include STEM characterization of the dispersed Pt species.

#### 3.2. Carbon surface oxidation

In this series of samples, the effect of oxidation of the carbon surface on Pt precursor dispersion after drying and Pt nanoparticle size after reduction is explored. An overlay of XRD patterns of Pt/KB300 samples (about 1 wt% Pt, or 0.1 atoms Pt/nm²) produced via SEA and subject to gas phase reduction at 170 °C is shown in Fig. 5a. The bottom pattern shows the support only, while the top pattern is for the hydrophobic, unoxidized carbon (PZC 10) synthesized with the anionic Pt hexachloride precursor at pH 2.9. (The anionic precursor was used for the unoxidized carbon since high PZC carbon supports do not adsorb cations [22], and it was desired to compare electrostatically adsorbed precursors.) The three center patterns for the PZC 6, 4, and 2 samples were synthesized with the cationic tetraamine precursor at pH 12.

Crystallinity in this series of samples is qualitatively seen, as in the section above, in the rise of the background between 30 and 50°20 arising from the most prominent Pt oxide peak and the first two fcc Pt peaks (the (111) at 39.8 and the (200) at  $46.2^{\circ}2\theta$ ). The highest degree of crystallinity appears to occur for the PZC 2 support, which is counter to the hypothesis that the more oxidized surface will lead to smaller nanodroplets of precursor and thus smaller nanoparticles. The other oxidized samples show a small degree of background rise, while the unoxidized sample shows the highest intensity of the Pt(111) peak. Background-subtracted fits of the four samples are shown in Fig. 5b. All fits require Pt oxide peaks in addition to Pt metal, as seen before [19-21], although the unoxidized sample shows the least amount of it, consistent with its larger particle size. Since all samples contain a significant fraction of Pt below the limit of detection of even this highly sensitive diffractometer, size trends from XRD will not be conclusive, and for a more accurate determination of particle size, STEM imaging was utilized.

Beyond an improved analysis of reduced particle size, STEM imaging was used to image the distribution of the SEA-adsorbed Pt precursor after drying. Shown in Fig. 6 are the SEA impregnated and dried samples

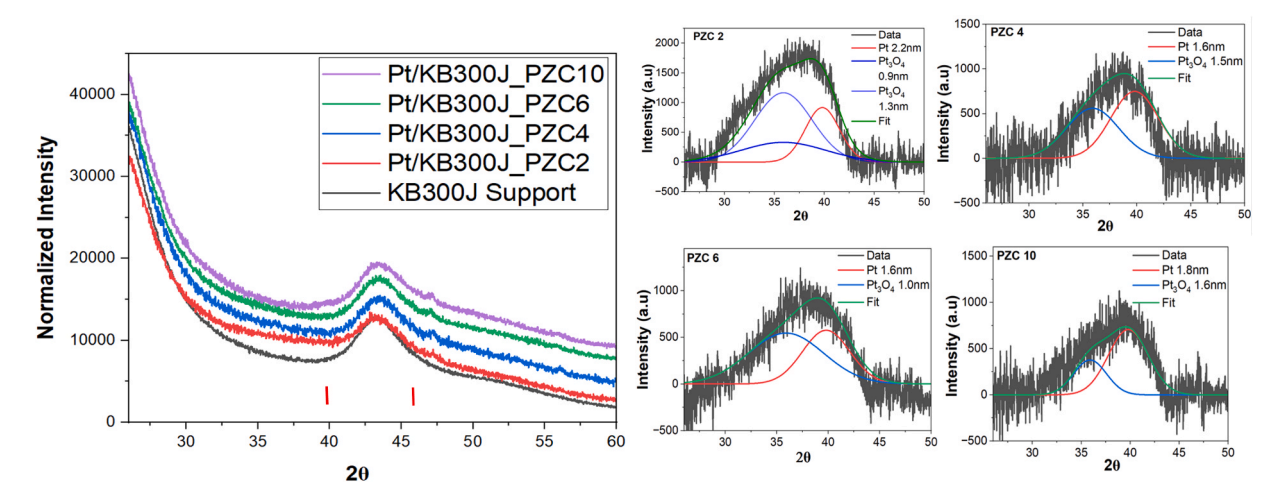


Fig. 5. a) XRD patterns of Pt nanoparticles over carbon substrates with various degrees of surface oxidation, b) Pt peak fits. Hashmarks indicate positions of fcc Pt peaks.

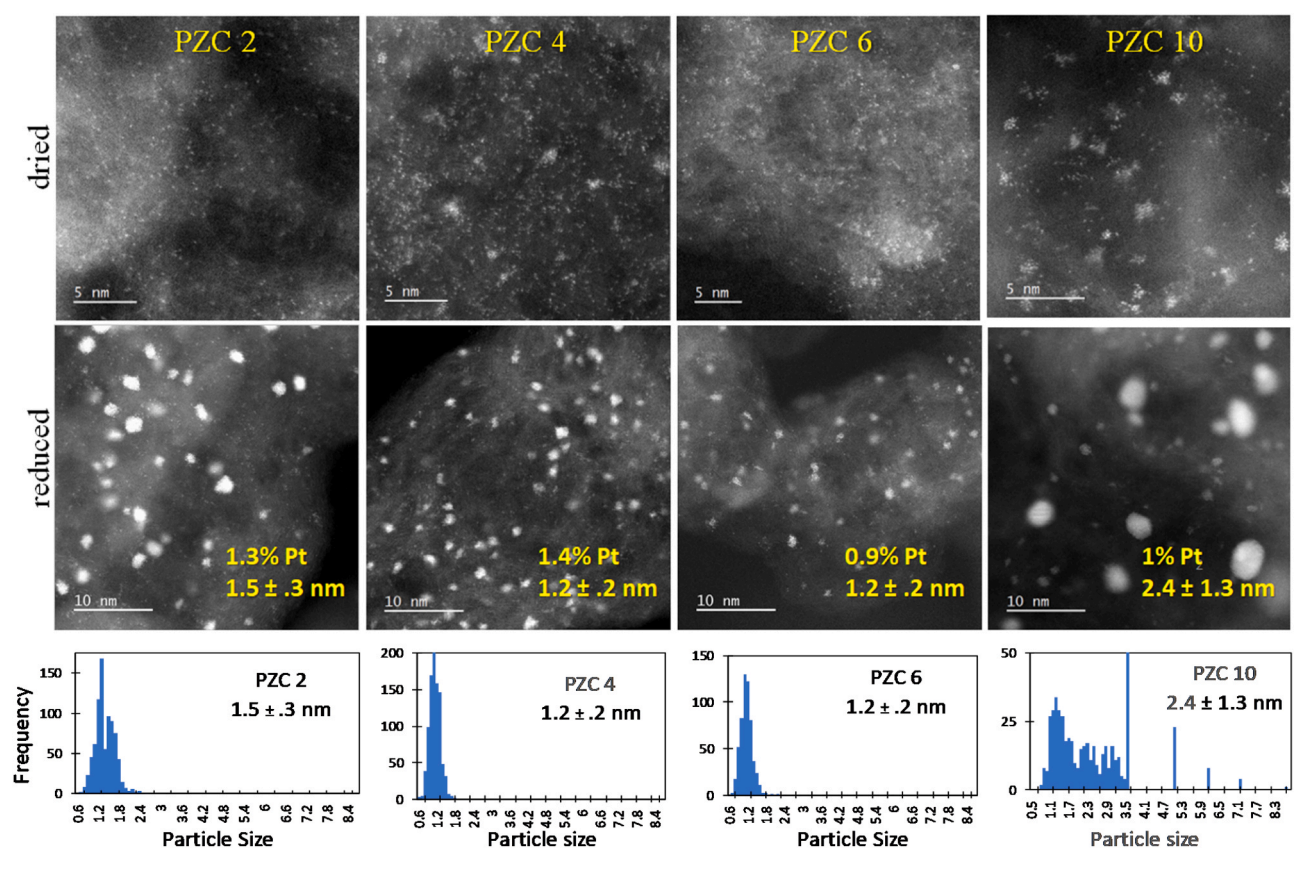


Fig. 6. STEM images and nanoparticle histograms of controlled hydrophilicity carbon supports.

(top row) and the gas phase reduced samples (bottom row) for the four Pt-containing samples. The dried, unoxidized (PZC 1) sample (top row, right) shows a high degree of precursor agglomeration as well as some isolated precursors, and as the surface oxidation become more severe

(moving right to left in the top row) the agglomeration of precursors appears to diminish until in the PZC 2 sample (top row, left), no agglomeration is seen. The original hypothesis that precursor agglomeration will decrease with increasing surface oxidation appears to be

**Table 1**Species fractions of atoms, dimers and trimers, and nanoparticles.

	PZC 2	PZC 4	PZC 6	PZC 10
	Isolated atoms = 81%↑	Isolated atoms = 52%↑	Isolated atoms = 51%↑	Isolated atoms = 33%
dried	Dim. and trimers = 19%	Dim. and trimers = 41%	Dim. and trimers = 39%	Dim. and trimers = 12%
	Nanoparticles = 0%↓	Nanoparticles = 7%↓	Nanoparticles = 10%↓	Nanoparticles = 55%
	Isolated atoms = 69%	Isolated atoms = 64% <b>↑</b>	Isolated atoms = 50%↑	Isolated atoms = 20%
reduced	Dim. and trimers = 20%	Dim. and trimers = 16%	Dim. and trimers = 23%	Dim. and trimers = 12%
	Nanoparticles = 11%↓	Nanoparticles = 21%↓	Nanoparticles = 28%↓	Nanoparticles = 68%

J.R. Regalbuto et al. Catalysis Today 431 (2024) 114556

correct through the drying stage at least, and is supported by a quantification of the STEM images into the fraction of isolated atoms, dimers and trimers, and nanoparticles shown in Table 1. As the PZC decreases, the fraction of isolated atoms increases and the fraction of "nanoparticles" (4 atoms clusters and above) decreases.

Volume-averaged particle size from the STEM images of the reduced samples given in the bottom row of images in Fig. 6 contain a more complete inventory of sub-nm nanoparticles and would thus be more accurate than XRD estimates. These show a decrease in reduced particle size with the moderate levels of surface oxidation, and in qualitative agreement with XRD, show an increase in reduced particle size of the PZC 2 sample. Perhaps the relatively high amount of surface oxygen causes relatively higher water evolution during reduction which causes sintering. It is notable, however, that as the surface is oxidized the fraction of nanoparticles goes down, and the fraction of isolated atoms increases all across the series. In sum, there may be an optimum in the degree of surface oxidation for obtaining highest overall metal dispersion; the highest degree of surface oxidation may cause sintering during the gas phase reduction.

A previous comparison of SEA-derived Pt particle size over unoxidized versus oxidized carbon xerogels [23] showed a slight increase of STEM-determined particle size for oxidized carbons prepared with cationic Pt versus unoxidized carbon with anionic Pt, 1.3 to 1.1 nm number average size, respectively. However, only one level of oxidation was used in that study, and the oxidation was extensive, yielding a PZC of close to 2. As suggested above, sintering due to high surface oxygen may have also occurred in this sample.

A more recent study reporting Pt particle size on oxidized versus unoxidized activated carbon supports [24] also showed a larger size (3.0 versus 2.4 nm number average), however that preparation was via incipient wetness with cationic Pt tetraammine, which would not be expected to interact strongly with the unoxidized carbon. There appears to be no other systematic comparison of the effect of surface oxidation on SEA-deposited Pt precursors.

### 3.3. Switched solvent synthesis

After a change in reduction chemistry in the first series of samples and a change in the surface chemistry in the second series above, in the

third series of samples the solvent is changed. A first set of results for SwiSS syntheses is presented in Fig. 7. Preparations of 0.5 wt% Pt/ VXC72 (0.1 atom/nm<sup>2</sup>) at three different acetone:water ratios, (4:1, 1:1, and 1:4) were dried at 50 °C (Fig. 7a) or 60 °C (Fig. 7b). Control experiments are given in the top three diffractograms of Fig. 7b; these are a physically mixed and 500 °C reduced precursor which gives 100% large particles (top pattern). This represents the diffractogram Pt peak intensity potentially present in each sample. The second pattern from the top is from a synthesis with the chloroplatinic acid precursor but without the solvent switch, making it akin to a "charge enhanced dry impregnation" (CEDI) preparation in which the protons from the acid precursor partially charge the surface of the carbon. This sample shows much smaller particles (3.0 nm) than the physically mixed precursor, but has about the same integrated intensity. Comparing the Pt peak intensities, and particularly the Pt (111) at  $39.8^{\circ}2\theta$ , of SwiSS-derived samples in this high sensitivity XRD data allows the qualitative determination that all or most of the Pt in these samples is very highly dispersed as undetectable clusters or atoms.

Patterns for the three acetone/water ratios dried at  $50\,^{\circ}\text{C}$  and reduced at 170, 300, and  $500\,^{\circ}\text{C}$  are shown in Fig. 7a. None of these samples shows appreciable crystallinity, even when reduced to  $500\,^{\circ}\text{C}$ . Fig. 7b includes three replicates at each acetone/water ratio, after drying at  $60\,^{\circ}\text{C}$  and reduction at the three temperatures. With the higher drying temperature, which is slightly higher than the boiling point of acetone ( $56.2\,^{\circ}\text{C}$ ), some crystallinity is noticeable in the 4:1 acetone: water ratios. (These were replicated an additional two times.) Interestingly, the peaks at all three reduction temperatures are about the same; it does not appear that sintering occurs at the higher reduction temperatures.

A second set of SwiSS preparations was performed with room temperature drying and 4.0 wt% Pt loading (0.5 atom/nm²) on the VXC72 support. Diffractograms of the physically mixed, high T-reduced, and CEDI control samples are given as the top two patterns in Fig. 8a. At the higher Pt loading the crystallinity of the reduced sample is quite sensitive to the acetone:water ratio. A survey of ratios between 5:1 and 1:2.75 is shown in Fig. 8b, and reveals an optimum ratio at about 2:1. Future work with these samples will include a determination of their stability at the higher reduction temperatures.

Perhaps the closest study in the literature to these SwiSS results is a

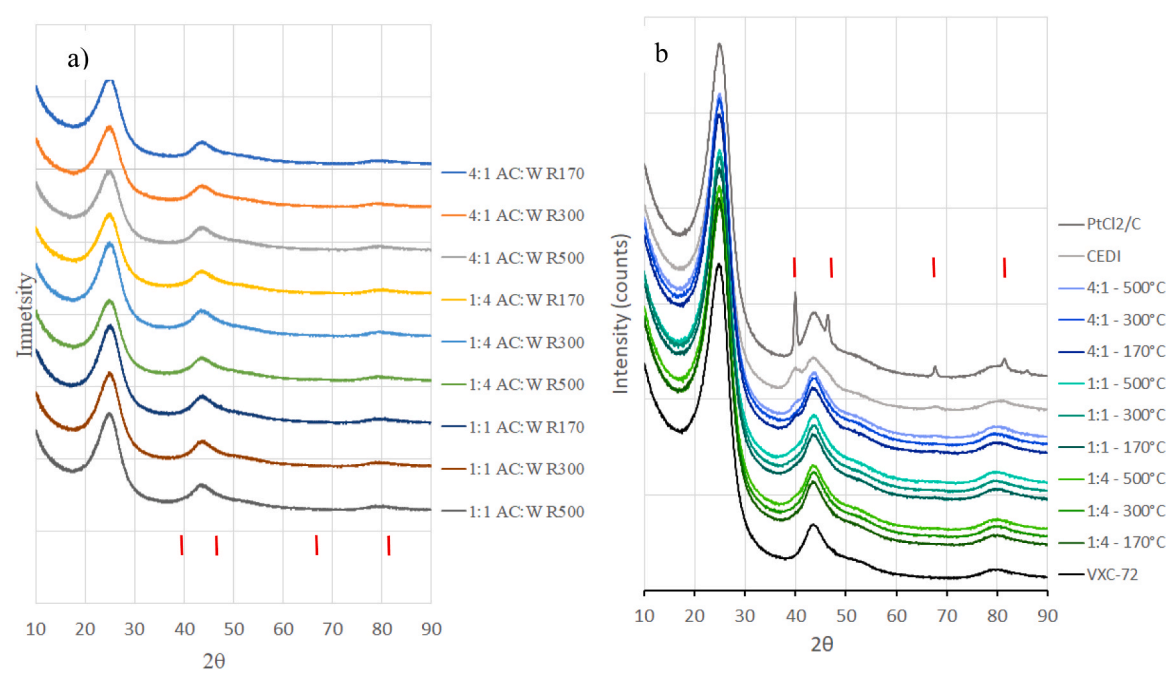


Fig. 7. XRD results for 0.5 wt% Pt/VXC72 dried at a) 50 °C and b) 60 °C. Hashmarks indicate positions of fcc Pt peaks.

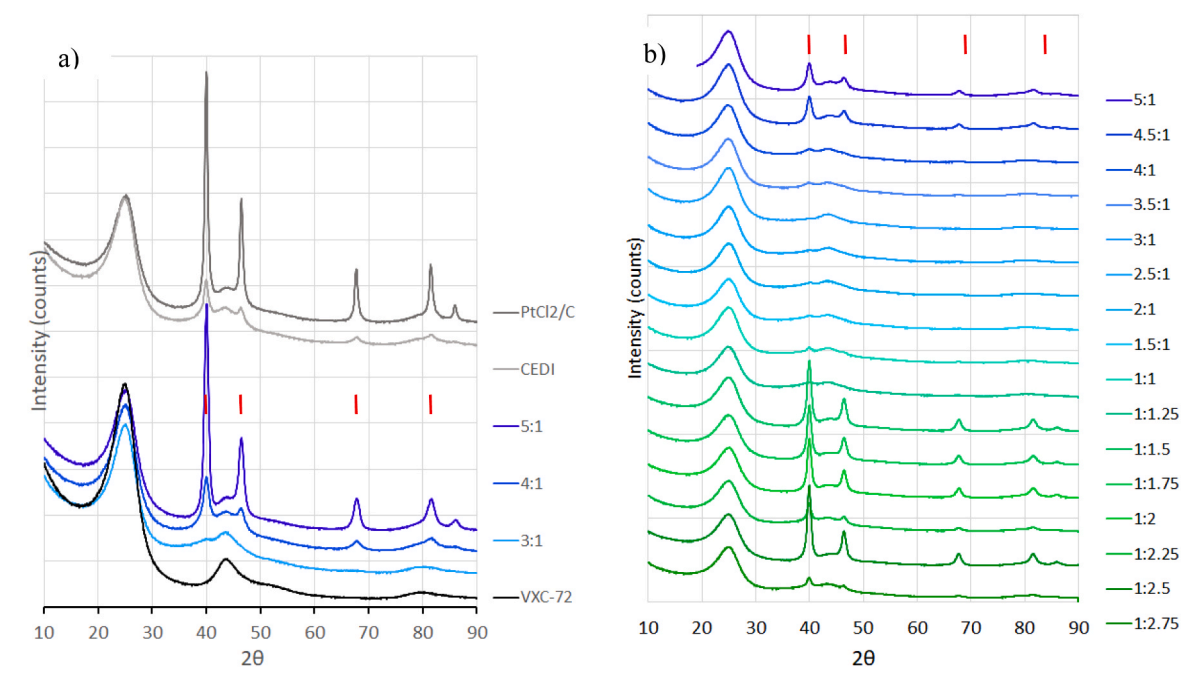


Fig. 8. XRD results for 4.0 wt% Pt/VXC72 dried at room temperature. Hashmarks indicate positions of fcc Pt peaks.

work in which solvents of decreasing polarity are employed in an effort to atomically disperse carbon supported gold and other noble metals [25]. Solvents of decreasing polarity and decreasing boiling point resulted in lower agglomeration of the precursors and the lowest polarity solvents such as acetone yielded isolated metal sites. No solvent switch was employed; metal precursors must be used which are soluble in the particular solvent employed. Solvents were kept free of water and interestingly, when syntheses with mixtures of acetone and water were attempted, higher fractions of water yielded larger particles. This is in contrast to the current observation of an optimum in the acetone:water ratio in solvent switching. Solvent switching also has the advantage of starting with a highly polar solvent in which most metal precursors are soluble.

Another group [26] has used short chain alcohols to decrease activated carbon supported zinc nanoparticle size from > 30 nm, where water was the sole solvent, to < 16 nm by adjusting the proportions of alcohols in the solvent mixture. This effect was attributed to the increased ability of the alcohols to wet the non-polar activated carbon surface, leading to better infiltration of the pore network and a higher metal dispersion. However, more significant lowering of polarity caused increased particle size, attributed to decreased solubility of the metal salt at polarities significantly lower than that of water, leading to agglomeration in solution.

While the powder XRD results demonstrate that SwiSS at optimum acetone:water ratios yields a supported metal phase more highly dispersed than can be achieved with charged enhanced (electrostatic) dry impregnation, the data reveal neither the detailed distribution of atoms and clusters, nor, more importantly, the mechanism by which acetone affects the drying. Future work on detailed characterization will be made by STEM and chemisorption to answer the first question, and separate experiments following the evolution of water and the wetting solvent from the powder during drying will be conducted in efforts to answer the second question.

## 4. Conclusions

In this work, three alternative methods have been employed to synthesize carbon supported Pt nanoparticles which are smaller than can be prepared by a "standard" method of strong electrostatic adsorption of charged Pt precursors followed by gas phase hydrogen reductions. In the first method, the gas phase reduction is replaced by a liquid phase reduction with hydrazine. Samples with 2 wt% Pt/VXC72 (0.3 atoms Pt/nm²) showed almost no crystallinity in high sensitivity XRD. Secondly, oxidizing a carbon black surface to render it more hydrophilic decreased the degree of agglomeration of Pt precursors after drying and yielded a higher percentage of isolated precursors. A highly oxidized, PZC 2 surface yielded 100% isolated precursors at 1.0 wt% Pt. The oxidized carbon surface yielded in general smaller average particle size than an unoxidized surface, but the high concentration of surface oxygen in the most oxidized surface did sinter the nanoparticles relative to the two intermediate levels of surface oxidation.

The third method involves a switch of solvent from water to acetone. Lower loading samples (0.5 wt% Pt or 0.1 atom Pt/nm²) on VXC72 carbon dried at 50 °C yielded samples with no detectable XRD signal at reduction temperatures up to 500 °C. At higher loadings of 4.0 wt%, dispersions of Pt higher than achievable by SEA were produced at acetone:water ratios of about 2:1.

The work presented here is a sampling of preliminary studies conducted in each of these three veins; separate, more detailed papers on each method are forthcoming.

#### CRediT authorship contribution statement

Chandler Edward: Data curation, Formal analysis. Ezeorah Chigozie: Data curation, Formal analysis, Writing – review & editing. Williams Christopher T.: Conceptualization, Funding acquisition, Writing – review & editing. Regalbuto John: Conceptualization, Writing – original draft, Writing – review & editing, Funding acquisition, Methodology. Jeon Tae-Yeol: Data curation, Formal analysis, Writing – review & editing. Gupton B. Frank: Data curation, Funding acquisition, Writing – review & editing. Pham Hien: Data curation. Datye Abhaya: Conceptualization, Writing – review & editing. Thornburg Nathan: Data curation, Formal analysis, Writing – review & editing. Romero Mikayla: Data curation, Formal analysis. Ojo Alaba: Data curation, Formal analysis, Writing – review & editing.

#### **Declaration of Competing Interest**

The authors declare the following financial interests/personal relationships which may be considered as potential competing interests: John R. Regalbuto reports financial support was provided by National Science Foundation.

#### **Data Availability**

Data will be made available on request.

#### Acknowledgements

This work was sponsored in part by NSF grant IIP 1939876 and NSF grant DUE 2050956.

#### References

- [1] J.P. Brunelle, Pure Appl. Chem. 50 (1978) 1211.
- [2] M.S. Heise, J.A. Schwarz, J. Coll. Interf. Sci. 107 (1985) 237.
- [3] M.S. Heise, J.A. Schwarz, J. Coll. Interf. Sci. 113 (1986) 55.
- [4] M.S. Heise, J.A. Schwarz, J. Coll. Interf. Sci. 123 (1988) 51.
- [5] Regalbuto, J.R., 2006. Surface and Nanomolecular Catalysis, Chapter 6: A Scientific Method to Prepare Supported Metal Catalysts, Richards, R. editor, Taylor and Francis/CRC Press, 2006.
- [6] Regalbuto, J.R., 2007. Catalyst Preparation: Science and Engineering, Chapter 13: Strong Electrostatic Adsorption of Metals onto Catalyst Supports, Regalbuto, J.R., ed., Taylor and Francis/CRC Press, 2007.

- [7] Regalbuto, J.R., 2009. Synthesis of Solid Catalysts, Chapter 3: Electrostatic Adsorption, de Jong, K., ed., Wiley-VCH Verlag, 2009.
- [8] S. Cao, J.R. Monnier, C.T. Williams, W.J. Diao, J.R. Regalbuto, J. Catal. 326 (2015) 69.
- [9] J.T. Miller, A.J. Kropf, M. Schreier, J.R. Regalbuto, J. Catal. 225 (2004) 203.
- [10] C. Park, P. Fenter, N. Sturchio, J.R. Regalbuto, Phys. Rev. Lett. 94 (2005) 076104/ 1.
- [11] J. Blanchard, A. Hervier, G. Costentin, J. Regalbuto, C. Louis, S. Boujday, Catal. Today 235 (2014) 245
- [12] N. Santhanam, T. Conforti, W. Spieker, J.R. Regalbuto, Catal. Today 21 (1994) 141.
- [13] B.L. Cushing, V.L. Kolenchenko, C.J. O'Connor, Chem. Rev. 104 (2004) 3893–3946.
- [14] H.C. Brown, C.A. Brown, J. Am. Chem. Soc. 84 (1962) 1494–1495.
- [15] C.P. Gibson, K.J. Putzer, Science 267 (1995) 1338-1340.
- [16] M.S. Makarov, S.N. Makarova, J. Phys.: Conf. Ser. 1369 (2019) 012056.
- [17] J.W. Park, E.H. Chae, S.H. Kim, J.H. Lee, J.W. Kim, S.M. Yoon, J.-Y. Choi, Mater. Chem. Phys. 97 (2006) 371–378.
- [18] X. Hao, L. Quach, J. Korah, J.R. Regalbuto, J. Mol. Catal. 219 (2004) 97.
- [19] R. Banerjee, Q. Liu, J.M.M. Tengco, et al., Detection of ambient oxidation of ultrasmall supported platinum nanoparticles with benchtop powder X-ray diffraction, Catal. Lett. 147 (2017) 1754–1764.
- [20] F.B.A. Rahman, H.N. Tien, H. Colon-Mercado, P. Ganesan, M.C. Elvington, J. B. Gaillard, S.G. Karakalos, J.R. Regalbuto, ACS Appl. Nano Mat. 5 (2022) 10292.
- [21] J. Lipp, R. Banerjee, M.F. Patwary, N. Patra, A.H. Dong, F. Girgsdies, S. Bare, J. R. Regalbuto, Chem. Mat. (2022), https://doi.org/10.1021/acs.chemmater.2c00101.
- [22] X. Hao, S. Barnes, J.R. Regalbuto, J. Catal. 279 (2011) 48.
- [23] S. Lambert, N. Job, L. D'Souza, M. Ribeiro Pereira, R. Pirard, B. Heinrichs, J. L. Figueiredo, J.P. Pirard, J.R. Regalbuto, J. Catal. 261 (2009) 23–33.
- [24] M. Führer, T. van Haasterecht, N. Masoud, D.H. Barrett, T. Verhoeven, E. Hensen, M. Tromp, C.B. Rodella, H. Bitter, ChemCatChem 14 (2022) e202200493.
- [25] X. Sun, S.R. Dawson, T.E. Parmentier, et al., Nat. Chem. 12 (2020) 560-567.
- [26] Z. Xu, M. Li, G. Shen, Y. Chen, D. Lu, P. Ren, H. Jiang, X. Wang, B. Dai, Nanomaterials 13 (3) (2023) 1–10.